NATIONAL ADVISORY COMMITTEE
FOR AERONAUTICS

TECHNICAL NOTE 3798

A THEORETICAL ESTIMATE OF THE EFFECTS OF COMPRESSIBILITY

ON THE PERFORMANCE OF A HELICOPTER ROTOR

IN VARIOUS FLIGHT CONDITIONS

By Alfred Gessow and Almer D. Crim

Langley Aeronautical Laboratory
Langley Field, Va.

NACA

AFMTC

TECH

NATIONAL ADVISORY COMMITTEE FOR AERONAUTICS

TECHNICAL NOTE 3798

A THEORETICAL ESTIMATE OF THE EFFECTS OF COMPRESSIBILITY

ON THE PERFORMANCE OF A HELICOPTER ROTOR

IN VARIOUS FLIGHT CONDITIONS
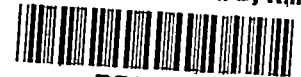
By Alfred Gessow and Almer D. Crim

SUMMARY

The effects of compressibility arising from high-tip-speed oper-
ation on the flapping, thrust, and power of a helicopter rotor over a
wide range of forward flight conditions are investigated by the use of
numerical methods.

For the particular set of airfoil characteristics used, the results
indicated minor increases in rotor flapping and thrust arising from
increasing rotor tip speed from 350 to 750 fps. The largest effect noted
was an increase in profile-drag power on the advancing side of the disk
that was proportional to the amount by which the blade-tip Mach number
exceeded the drag-divergence Mach number. These effects of compressi-
bility appeared to be independent of blade twist but are, of course, a
function of the airfoil characteristics employed in the analysis.

INTRODUCTION

Helicopter design trends during the past few years have been in the
direction of using higher rotor tip speeds. Thus, whereas the tip speeds
of early production helicopters were as low as 450 fps, current models
are being built with tip speeds of the order of 700 fps and even higher.
This trend towards high speeds results from the use of higher disk
loadings in today's larger helicopters, from the use of various tip-
propulsion systems, and from the desire to achieve higher helicopter
forward speeds.

Except for reference 1, which presents the results of an investi-
gation of the effects of compressibility on rotor profile-drag power in
hovering, experimental data dealing with the effect of high tip speeds
on helicopter performance and limiting forward speeds are very meager.
Although such items as vibration and control limitations on forward
speed arising from compressibility must await experimental investigation,

it is possible, pending experimental verification, to obtain an estimate of the effect of compressibility on such performance items as rotor flapping, thrust, and power by theoretical means. The reasonableness of such an approach has been indicated by the obtaining of a fair comparison between the data of reference 1 and theoretical curves utilizing two-dimensional compressible airfoil data in standard hovering equations.

Consequently, in order to provide helicopter designers with an estimate of the effects of high rotor-tip-speed operation on rotor performance, a series of numerical calculations were carried out. In the calculations, an assumed set of two-dimensional compressible airfoil data was utilized in conjunction with the equations and procedures outlined in reference 2 for obtaining the flapping, thrust, and power of a rotor operating at several values of tip speed and at tip-speed ratios ranging from 0.2 to 0.5. The results of the study, which are dependent on the particular set of airfoil characteristics assumed, are presented herein.

SYMBOLS

a_0 constant term in Fourier series that expresses β; hence, rotor coning angle

a_n coefficient of $\cos n\psi$ in Fourier series that expresses β

b number of blades per rotor

b_n coefficient of $\sin n\psi$ in expression for β

B tip-loss factor; blade elements outboard of radius BR are assumed to have profile drag but no lift

c blade section chord at radial station r, ft

c_d section drag coefficient

c_e equivalent blade chord (weighted on thrust basis),
$$\frac{\displaystyle\int_0^R cr^2\,dr}{\displaystyle\int_0^R r^2\,dr},\ \text{ft}$$

c_l section lift coefficient

C_T rotor thrust coefficient, $\dfrac{T}{\pi R^2 \rho (\Omega R)^2}$

C_P rotor-shaft power coefficient, $\dfrac{P}{\pi R^2 \rho (\Omega R)^3}$

$\Delta \dfrac{C_{P,o}}{\sigma}$ increment in rotor profile-power-coefficient—solidity ratio arising from compressibility effects

I_h mass moment of inertia of blade about flapping hinge, slug-ft^2

M_d drag-divergence Mach number of blade sections

ΔM_d amount by which the Mach number of advancing blade tip ($\psi = 90°$) exceeds Mach number for drag divergence of two-dimensional airfoil at angle of attack corresponding to that at blade tip

P rotor-shaft power, ft-lb/sec

r radial distance from center of rotation to blade element, ft

R blade radius measured from center of rotation, ft

T rotor thrust, lb

u nondimensional resultant velocity perpendicular to blade-span axis at blade element

u_T component at blade element of u perpendicular to blade-span axis and to axis of no feathering

x ratio of blade-element radius to rotor-blade radius, r/R

v induced velocity at rotor (always positive), fps

V true airspeed of helicopter along flight path, fps

α rotor angle of attack; angle between axis of no feathering (that is, axis about which there is no cyclic-pitch change) and plane perpendicular to flight path, positive when axis is inclined rearward, deg

α_r section angle of attack at radial position r, deg

$\alpha_{(x)(\psi)}$ blade-element angle of attack at any radial position x and at any blade azimuth angle ψ, (for example, $\alpha_{(1.0)(270^\circ)}$ is blade-element angle of attack at tip of retreating blade at 270° azimuth position), deg

β blade flapping angle with respect to no-feathering axis at a particular azimuth position, radians

γ' mass constant of rotor blade, $c_e \rho R^4 / I_h$

$\theta_{.75}$ blade-section pitch angle at 0.75 radius; angle between line of zero lift of blade section and plane perpendicular to axis of no feathering, deg

$\theta_{.75B}$ blade-section pitch angle at 0.75B radius, deg

θ_1 difference between hub and tip pitch angles, positive when tip angle is larger, deg

λ inflow ratio, $\dfrac{V \sin \alpha - v}{\Omega R}$

μ tip-speed ratio, $V \cos \alpha / \Omega R$

ρ mass density of air, slugs/cu ft

σ rotor solidity, $b c_e / \pi R$

ψ blade azimuth angle measured from downwind position in direction of rotation, deg

Ω rotor angular velocity, radians/sec

Subscripts:

adv   advancing side of rotor disk

o   profile

u   useful

METHOD AND SAMPLE CASES

Method of Analysis

The numerical-integration method of reference 2 necessarily uses λ, $\theta_{.75}$, and μ as the primary input variables and computes as

an output such items as thrust, torque, power, and so forth. Other than by an iterative process, it is not possible to reverse the procedure, that is, to start with thrust, power, and tip-speed ratio and solve for λ and $\theta_{.75}$. The effects of compressibility on the characteristics of rotors can be compared on the basis of keeping λ, $\theta_{.75}$, and μ constant or, perhaps more desirably, on the basis of keeping C_T, $\left(C_P/C_T\right)_u$, and μ constant. In order to keep the computation time to a minimum, the examples contained herein are compared on the basis that λ, $\theta_{.75}$, and μ are constants. At each μ value, however, λ and $\theta_{.75}$ were varied in a manner that resulted in values of C_P/σ which ranged from very low (close to autorotation) to very high (full power) at approximately constant C_T/σ.

In each case, the numerical integrations were effected by calculating the section contributions at six radial and eight azimuth stations. As discussed in reference 2, this number of stations was found to yield substantially the same answers as obtained by using larger numbers. Rotor inflow was assumed to be uniform over the disk.

Assumed Flight Conditions and Sample Rotor

The effects of compressibility were determined by computing, for given combinations of λ, $\theta_{.75}$, and μ, various rotor characteristics at several different tip-speed values and then comparing the results obtained at high and low tip speeds. Most of these comparisons were made between a "base" tip-speed value of 350 fps (low enough to be essentially free of compressibility effects) and a higher value of 750 fps, although a few computations were also made at 650 fps and 900 fps. This range of tip speeds, together with tip-speed ratios from 0.2 to 0.5, resulted in a range of Mach numbers from about 0.27 to nearly 1.0 at the tip of the advancing blade.

In this analysis the physical characteristics of the rotor were held constant, with the exception of blade twist. These characteristics included a mass factor γ' of 1.0, untapered blades, zero flapping-hinge offset, and a blade root cutout of 0.15R. Although most of the cases were computed for blades having -8° of twist, a limited comparison is made with blades having 0° and -16° twist.

Assumed Airfoil Data

Airfoil section lift and drag values over a wide range of angles of attack and Mach numbers are required when blade compressibility and stall are to be included in a rotor analysis. Although such data are usually

not available at angles of attack much beyond the stall, reference 3 gives
the results of four symmetrical NACA 6-series airfoils tested at angles
of attack from -2° to 31° and at Mach numbers from 0.3 to about 0.85.
For the present calculations, which were performed by automatic computing
machines, the data of this reference corresponding to the NACA 64_1-012
airfoil were roughly approximated by constructing a series of lift and
drag curves composed of short straight-line segments. The Mach number
range between approximately 0.85 and 1.0, which is not covered in ref-
erence 3, was extrapolated with the aid of unpublished data for an air-
foil of the same thickness. The airfoil data used are shown in figure 1.

The airfoil selected (12 percent) is somewhat thicker than would be
chosen from compressibility considerations alone but is comparable to
those currently in use for helicopter blades except for the lower than
usual stall angle (approximately 8.5°). Thus, the effects of compress-
ibility on rotor aerodynamic characteristics that are indicated in sub-
sequent sections of this paper would be somewhat greater than expected
in actual operation when thinner blades are used. In addition, no
attempt was made to take into account the alleviating "three-dimensional"
effect of the blade tips on the section coefficients in the region of the
blade tips. (As mentioned in ref. 1, propeller data have shown the drag-
divergence tip Mach number to be about 0.06 above the two-dimensional
results, and a similar trend was shown for the case of the hovering
rotor.)

RESULTS

Figures 2 through 5 show the flapping coefficients, thrust-coefficient—
solidity ratios C_T/σ, profile-power—thrust coefficient ratios $C_{P,o}/C_T$,
and power-thrust coefficient ratios C_P/C_T as computed for rotor tip
speeds of 350 and 750 fps for tip-speed ratios ranging from 0.2 to 0.5.
The combinations of the input variables λ, $\theta_{.75}$, and μ represent a
wide range of flight conditions at an approximately constant thrust
coefficient.

Flapping Coefficients

The flapping coefficients shown in figures 2(a), 3(a), 4(a),
and 5(a) indicate relatively small changes due to compressibility.
Although in all cases the coefficients are higher for operation at a
tip speed of 750 fps, the actual increases are usually not large. For
example, the coning angle a_0 is typically only 0.3° to 0.4° higher
for the higher tip speed while the first-harmonic coefficients a_1

and b_1 show increases ranging, respectively, from 0.3° to 1.5° and from 0.2° to 0.3°.

Thrust

The effect of compressibility on thrust is to increase the thrust-coefficient—solidity ratio, as shown in figures 2(b), 3(b), 4(b), and 5(b). This increase, which is about 10 percent in most cases, apparently is a result of the higher lift-curve slopes at higher Mach numbers. Although the lift-curve slope is sharply reduced at a Mach number of about 0.8, the thrust is not noticeably affected for cases where such a condition occurs. This may be explained by the fact that the section angles of attack in the vicinity of the blade tip near the 90° azimuth position (where the higher Mach numbers occur) are very low; consequently, a reduction in lift-curve slope has little significance. In addition, the percentage contribution of this region to the total rotor thrust is relatively small.

Power

The profile-drag power losses, as would be expected, are substantially increased by increasing the tip speed from 350 to 750 fps. The magnitude of these losses is shown in figures 2(b), 3(b), 4(b), and 5(b) in the form of profile-power—thrust coefficient ratios $C_{P,o}/C_T$ for the two tip speeds concerned. The difference between the two represents compressibility effects and is smallest at the lowest tip-speed ratio 0.2 and increases with increasing values of μ. At $\mu = 0.4$, the profile-drag power losses at 750 fps are approximately double those at 350 fps.

The power-thrust coefficient ratios C_P/C_T are also shown in order to illustrate the wide range of flight conditions covered. Zero values of C_P/C_T indicate an autorotating rotor, negative values indicate that the rotor is supplying power, and positive values indicate the normal condition where power is being absorbed by the rotor. The difference between the curves of 350 and 750 fps simply reflects, in large part, the differences already noted in the $C_{P,o}/C_T$ curves.

For performance estimations, a more convenient form of representation of the profile-drag power losses due to compressibility is shown in figure 6. Here, the difference in the profile-power-coefficient—solidity ratio between the base tip speed of 350 fps and the higher tip speeds is shown as a function of the amount by which the drag-divergence Mach number has been exceeded at the tip of the advancing blade. The points shown represent a range of tip-speed ratios from 0.2 to 0.5, thrust-coefficient—solidity ratios from about 0.035 to 0.08, blade

twists of 0°, -8°, and -16°, and flight conditions from near autorotation to very high power. As shown in figure 1(b), the drag-divergence Mach number for this airfoil was approximately 0.75 for the small angles of attack that are typical of the advancing-blade tip.

Since the parameter ΔM_d shown in figure 6 applies only to the advancing side of the rotor and since it is possible for compressibility losses to also occur on the retreating side, the differences in profile-drag power losses were computed for the advancing side of the disk only and are shown in figure 7. Although the scatter is somewhat reduced, the faired curve is only slightly lower than that of figure 6 and indicates that the advancing side accounts for most of the compressibility losses for the cases studied.

In reference 4, a somewhat different method of predicting compressibility losses was employed which includes the profile-drag losses at 0° azimuth as well as at 90°. When this method was applied to the present data, a comparable amount of scatter to that shown in figure 6 resulted, possibly because of the much wider range of variables covered in the calculations of this paper. It is possible, however, that for some other types of airfoil characteristics the use of two azimuth positions might give better results than the single value which was found to be adequate in this paper.

Blade stalling may also contribute substantially to profile-drag power losses (ch. 10 of ref. 5, for example), and when compressibility effects are also present the losses due to each source are difficult to separate. Some idea of the relative magnitudes of such losses may be gained from plots similar to those of figure 8, which show the radially integrated power loss at each azimuth position as computed for tip speeds of 350 and 750 fps. Losses due to stalling appear as a peak in the curve for 350 fps near the azimuth position (310°) corresponding to the highest local section angle of attack, which in this case was about 5° beyond the stall. Compressibility losses, represented by the difference between the two curves, are at a maximum on the advancing blade where the relative velocity is greatest. For this case, it may thus be seen that the compressibility losses on the advancing side are far greater than the stall losses on the retreating side.

The curves for $C_{P,o}/C_T$ and C_P/C_T shown in figures 2(b), 3(b), 4(b), and 5(b) include losses from both stalling and compressibility. However, the difference between the curves for tip speeds of 350 and 750 fps, shown also as $\Delta \dfrac{C_{P,o}}{\sigma}$ in figure 6, can be attributed almost entirely to compressibility effects inasmuch as the section angles of attack differed only negligibly for the two tip speeds. Figure 6 could therefore be used to estimate compressibility losses for rotors having

similar airfoil characteristics to those used in the present calcu-
lations. Somewhat different results might be expected for rotor blades
whose variation of drag-divergence Mach number with section angle of
attack is not as flat as that shown in figure 1(a). (An example of a
steeper variation is shown in fig. 7 of ref. 1.) Stall losses could be
considered separately by the methods discussed in reference 4 or 5.
Compressibility and stall losses may be added to basic values (obtained,
for example, from the charts of refs. 6 and 7) which do not include
stall or compressibility effects.

Twist

The previous discussion has been based on results obtained with
blades having a twist of $-8°$. In order to determine the effects of
twist at high tip speeds, the calculations were repeated for blade twists
of $0°$ and $-16°$ for the combinations of input variables used in figure 4
($\mu = 0.4$, $\Omega R = 750$ fps). Blades having different twists are usually
compared on the basis of equal pitch at $0.75R$ and this procedure is
followed in the present case. In figure 9 the thrust-coefficient—
solidity ratios, power-thrust coefficient ratios, flapping coefficients,
and tip angles of attack are plotted against $\theta_{.75}$ for the three twist
values of $0°$, $-8°$, and $-16°$. Examination of this figure shows that
although the flapping coefficients are little affected by twist, the
thrust-coefficient—solidity ratios are significantly higher for the
twisted blades. These thrust differences would be cut approximately in
half if C_T/σ for the different twist values were computed at the same
value of $\theta_{.75B}$ instead of at constant $\theta_{.75}$.

Figure 10 shows the radial thrust distribution obtained by averaging
the values around the azimuth for the case of $\theta_{.75} = 8°$ in figure 9.
Although the twisted blades exhibit a lower thrust near the tips, because
of the lower tip angles of attack, the increased thrust loading inboard
more than offsets this loss. In a similar manner, the radially inte-
grated thrust plotted in figure 11 for various azimuth positions (for the
same flight conditions shown in fig. 10) shows that the greatest differ-
ences in thrust and in power are on the advancing blade, with the highest
twist having the largest thrust but also the greatest profile-drag power
loss. In the higher collective-pitch range, however, figure 9 shows an
advantage in profile-power efficiency for the twisted blades over the
untwisted ones as indicated by lower $C_{P,o}/C_T$ ratios. This advantage is
of a greater order of magnitude than that resulting from the reduction
of $C_{P,o}/C_T$ that occurs when operating at a higher C_T/σ.

The tip angles of attack on both the advancing and retreating sides
of the disk are shown in figure 9(c) and, as would be expected, are lower

for the twisted cases. The difference between twists of 0° and -16° is
seen to be about 4.5° on the advancing side and about 2.5° on the retreating
side. The difference in retreating-blade-tip angles of attack would be
about 4.5° (instead of 2.5°) if the 0° and -16° twist blades were com-
pared on the basis of the same C_T/σ. On such a basis, the difference
in advancing-blade-tip angles of attack would remain unchanged at about
4.5°, inasmuch as these angles are relatively insensitive to changes
in C_T/σ at the higher advance ratios.

The twist effects discussed were based on an assumed tip speed
of 750 fps. In order to compare the effects of compressibility for var-
ious values of twist, some additional cases were computed using a tip
speed of 350 fps, and the results are shown in figure 12. Although the
effects of compressibility are clearly evident in the increased power
and thrust ratios, these increases are almost identical for the 0°, -8°,
and -16° twists.

<p style="text-align:center">Comparison With Charts</p>

Because of the length and complexity of equations relating to heli-
copter performance, charts such as those of references 6, 7, and 8 are
usually employed for performance calculations. Although such charts have
been found to provide a rapid yet accurate method of estimating the per-
formance of conventional helicopters, they do not take stall or com-
pressibility into account. Therefore, it is of interest to compare some
results obtained by the numerical method with those from the reference
charts in order to determine the extent of agreement.

The degree to which the charts would be in error because of their
omission of compressibility effects can be obtained from the discussion
of the preceding sections of this paper; the differences between the
350 fps and the higher tip-speed cases represent the error involved.
When the values obtained by the numerical method for a tip speed of
350 fps are compared with chart values, however, the differences between
the two methods will be due almost entirely to stalling, except for small
differences resulting from somewhat different airfoil characteristics
below the stall. Figure 13 shows the thrust-coefficient—solidity
ratio C_T/σ, profile-power—thrust ratio $C_{P,o}/C_T$, and flapping coeffi-
cients as obtained by the two methods for a tip-speed ratio of 0.3. In
addition, the section angles of attack on the retreating blade ($\psi = 270^\circ$)
at the tip and at the radial station where $u_T = 0.4$ are also shown in
order to illustrate the degree of tip and inboard stalling. As shown in
the figure, the stall angle for this particular airfoil (at low Mach num-
bers) was about 8.5°.

The flapping coefficients as obtained by the two methods are shown
in figure 13(a). The agreement is generally good except for conditions

involving large amounts of stall. The coning angle a_0 is seen to be reduced by stalling, whereas the other coefficients increase as stalling increases.

Examination of figure 13(b) shows good agreement between the two methods for the thrust-coefficient—solidity ratio and reasonably good agreement for the profile-power—thrust ratio for conditions where little stall is present. (Very close agreement would be expected if the same airfoil characteristics below the stall were used in both methods.) For the higher values of pitch, however, where the tip angle of attack substantially exceeds the stall angle, the charts underestimate the profile-drag power losses. Poorer agreement is also evident at the very low pitch angles (corresponding to low power or autorotation) where inboard stalling is present.

A similar comparison between rotor characteristics computed by the numerical and analytical methods at other tip-speed ratios leads to similar conclusions. At lower tip-speed ratios, for example, wherein somewhat less stall is present, the agreement between the two methods is close and holds over a wider range of pitch angles. At higher tip-speed ratios, such as 0.4 and 0.5, the larger amount of stall causes somewhat poorer agreement than is shown for the case of $\mu = 0.3$.

It is thus concluded that the charts of references 6, 7, and 8 can be used in place of numerical calculations for flight conditions involving little rotor compressibility and stall and can provide a base value for the rapid estimation of rotor flapping, thrust, and power under conditions involving compressibility and stall.

CONCLUDING REMARKS

A numerical study was made of the effect of compressibility on the flapping, thrust, and torque of a sample rotor over a wide range of forward flight conditions. The sample rotor was assumed to have untapered blades with constant-thickness airfoil sections that were represented by a specific set of two-dimensional lift and drag characteristics that varied with Mach number. The application of these data in the assumed flight conditions resulted in the following effects, which are dependent in large measure on the particular set of airfoil characteristic used.

1. Increasing the tip speed from 350 fps to 750 fps resulted in minor increases in the rotor flapping and thrust coefficients. The largest flapping increases, ranging from 0.3° to 1.5°, occurred in the first-harmonic longitudinal flapping; the thrust-coefficient increase was of the order of 10 percent.

2. The increases in profile-drag power associated with increasing tip speeds and tip-speed ratios occurred primarily on the advancing side of the disk and appeared to be a function of the amount by which the Mach number of the tip of the advancing blade exceeds the drag-divergence Mach number corresponding to the tip angle of attack.

3. The increases in rotor flapping, thrust, and profile-drag power resulting from compressibility effects appeared to be independent of blade twist.

4. A rapid estimation of rotor flapping, thrust, and power under conditions involving compressibility and stall can be made by using the indications of this paper together with standard analytical rotor theory.

Langley Aeronautical Laboratory,
       National Advisory Committee for Aeronautics,
              Langley Field, Va., June 11, 1956.

REFERENCES

1. Carpenter, Paul J.: Effects of Compressibility on the Performance of Two Full-Scale Helicopter Rotors. NACA Rep. 1078, 1952. (Supersedes NACA TN 2277.)

2. Gessow, Alfred: Equations and Procedures for Numerically Calculating the Aerodynamic Characteristics of Lifting Rotors. NACA TN 3747, 1956.

3. Wilson, Homer B., Jr., and Horton, Elmer A.: Aerodynamic Characteristics at High and Low Subsonic Mach Numbers of Four NACA 6-Series Airfoil Sections at Angles of Attack From -2° to 31°. NACA RM L53C20, 1953.

4. Amer, Kenneth B.: Effect of Blade Stalling and Drag Divergence on Power Required by a Helicopter Rotor at High Forward Speed. Proc. Eleventh Annual Forum, Am. Helicopter Soc., Inc., April 27-30, 1955, pp. 100-109.

5. Gessow, Alfred, and Myers, Garry C., Jr.: Aerodynamics of the Helicopter. The Macmillan Co., c.1952.

6. Gessow, Alfred, and Tapscott, Robert J.: Charts for Estimating Performance of High-Performance Helicopters. NACA TN 3323, 1955.

7. Tapscott, Robert J., and Gessow, Alfred: Supplementary Charts for Estimating Performance of High-Performance Helicopters. NACA TN 3482, 1955.

8. Tapscott, Robert J., and Gessow, Alfred: Charts for Estimating Rotor-Blade Flapping Motion of High-Performance Helicopters. NACA TN 3616, 1956.
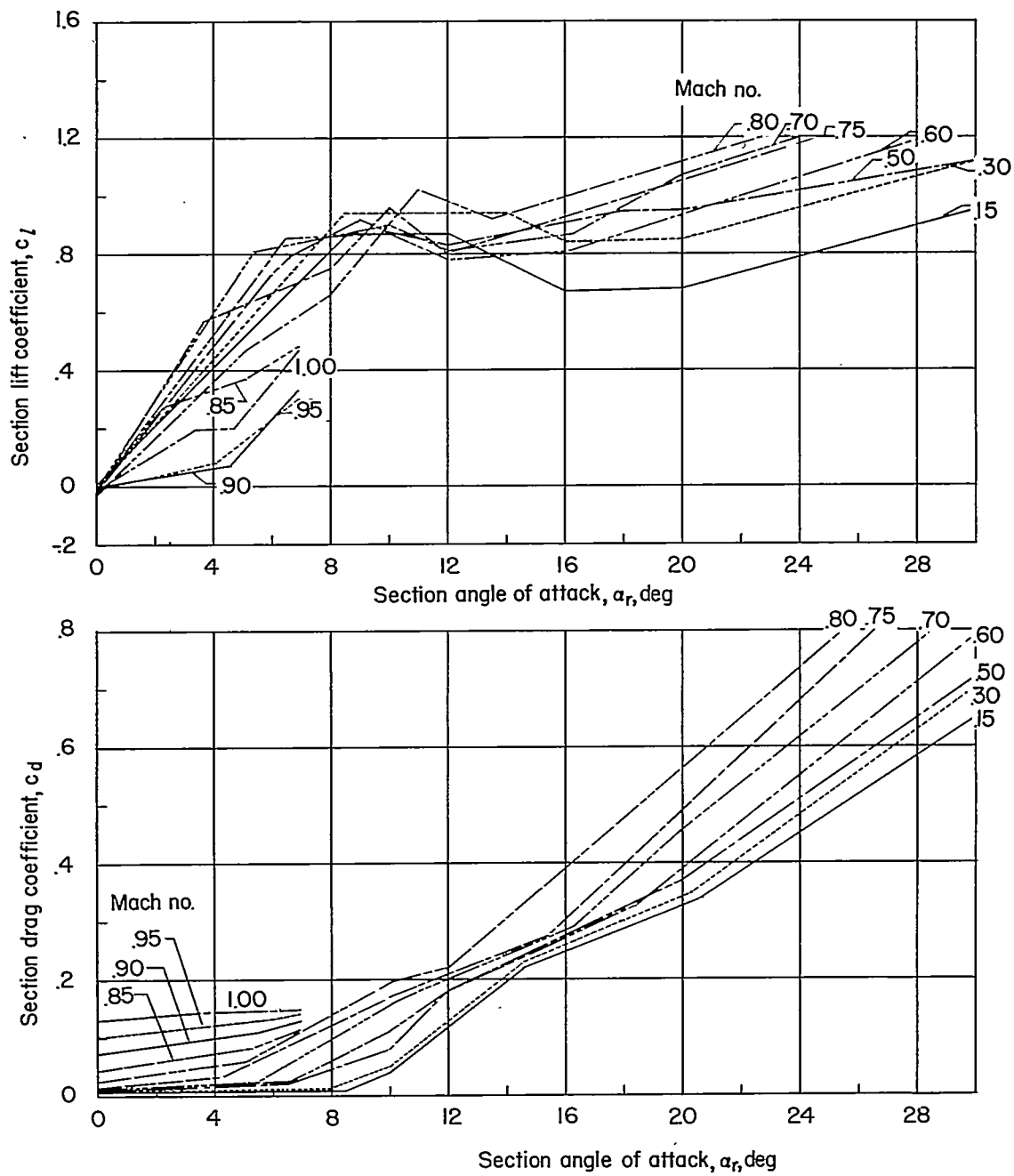
(a). Section lift and drag data.

Figure 1.- Airfoil data used in numerical calculations.

$$\alpha_r, \text{deg}$$
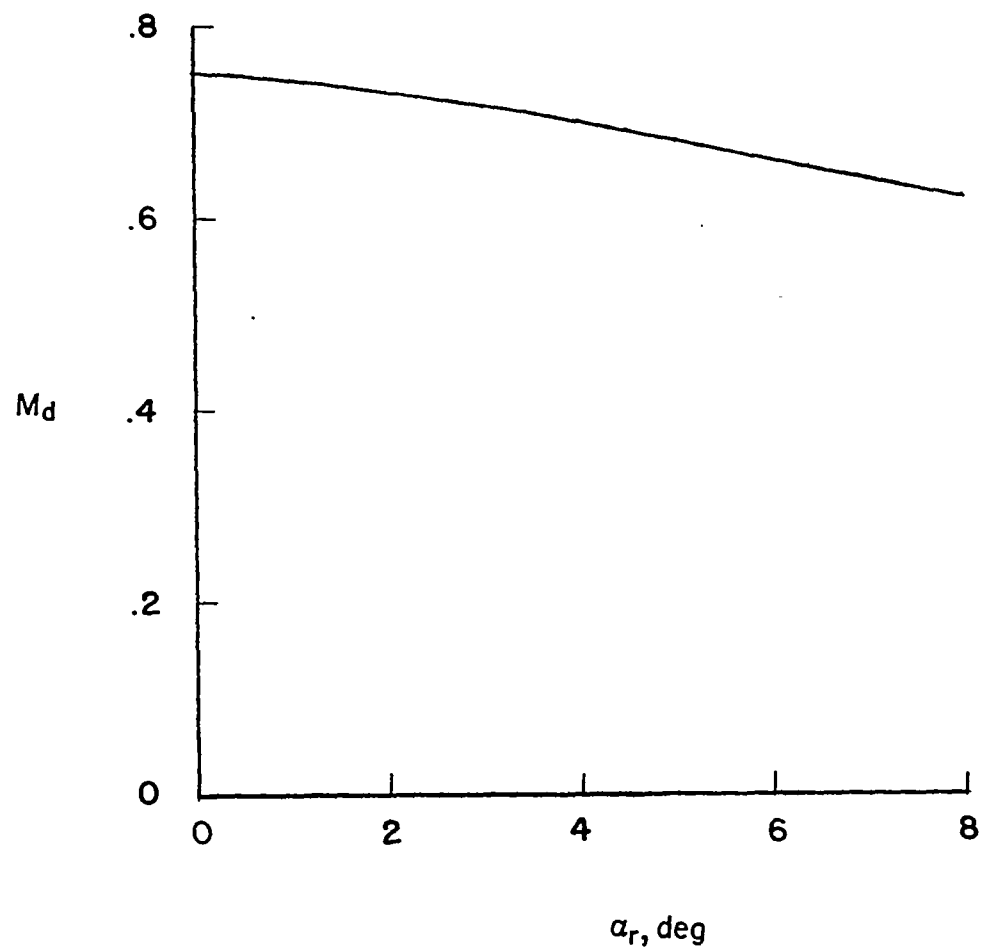
(b) Drag-divergence Mach number plotted against section angle of attack.

Figure 1.- Concluded.
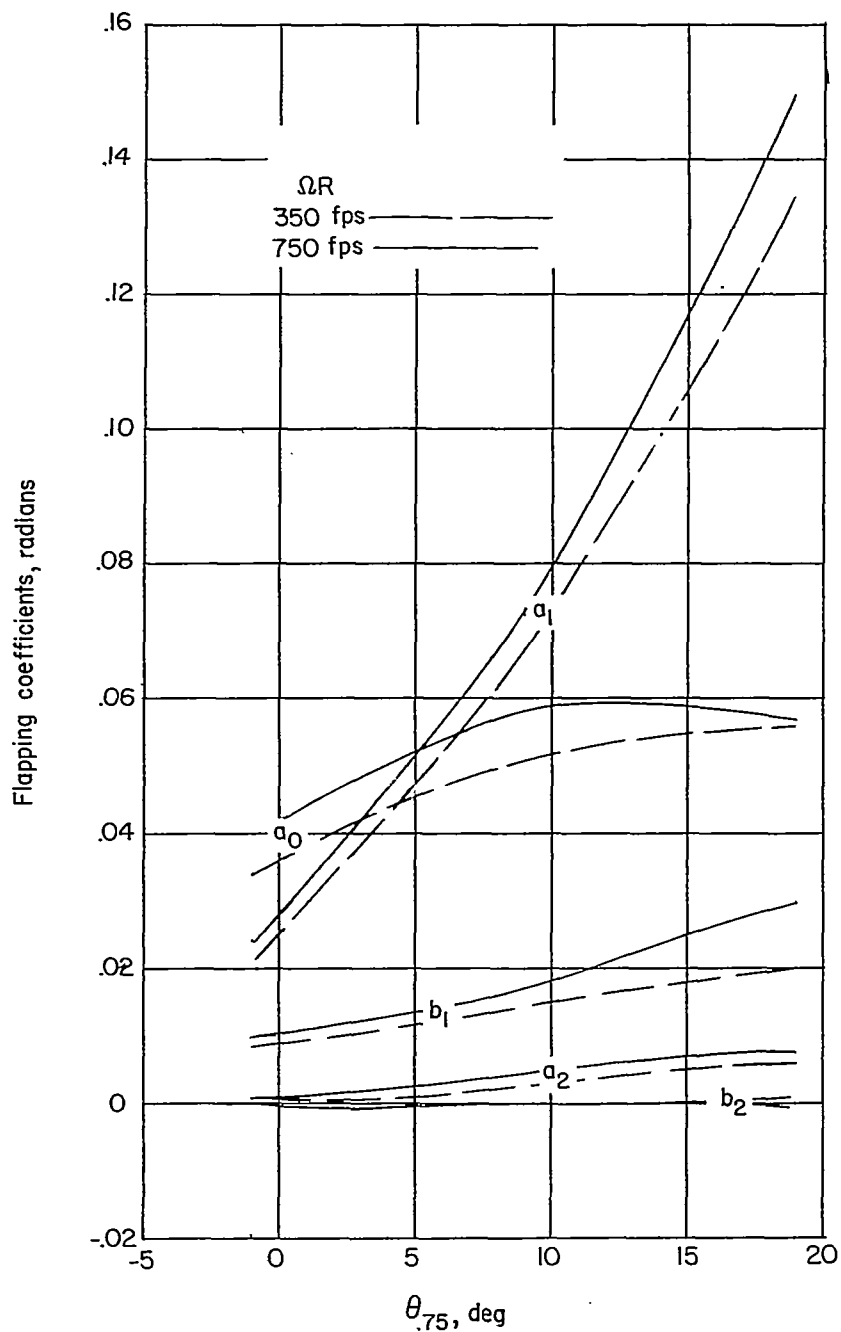
(a) Flapping coefficients.

Figure 2.- Aerodynamic effects of high-tip-speed operation $\left(\mu = 0.2, \quad \theta_1 = -8^\circ\right)$.
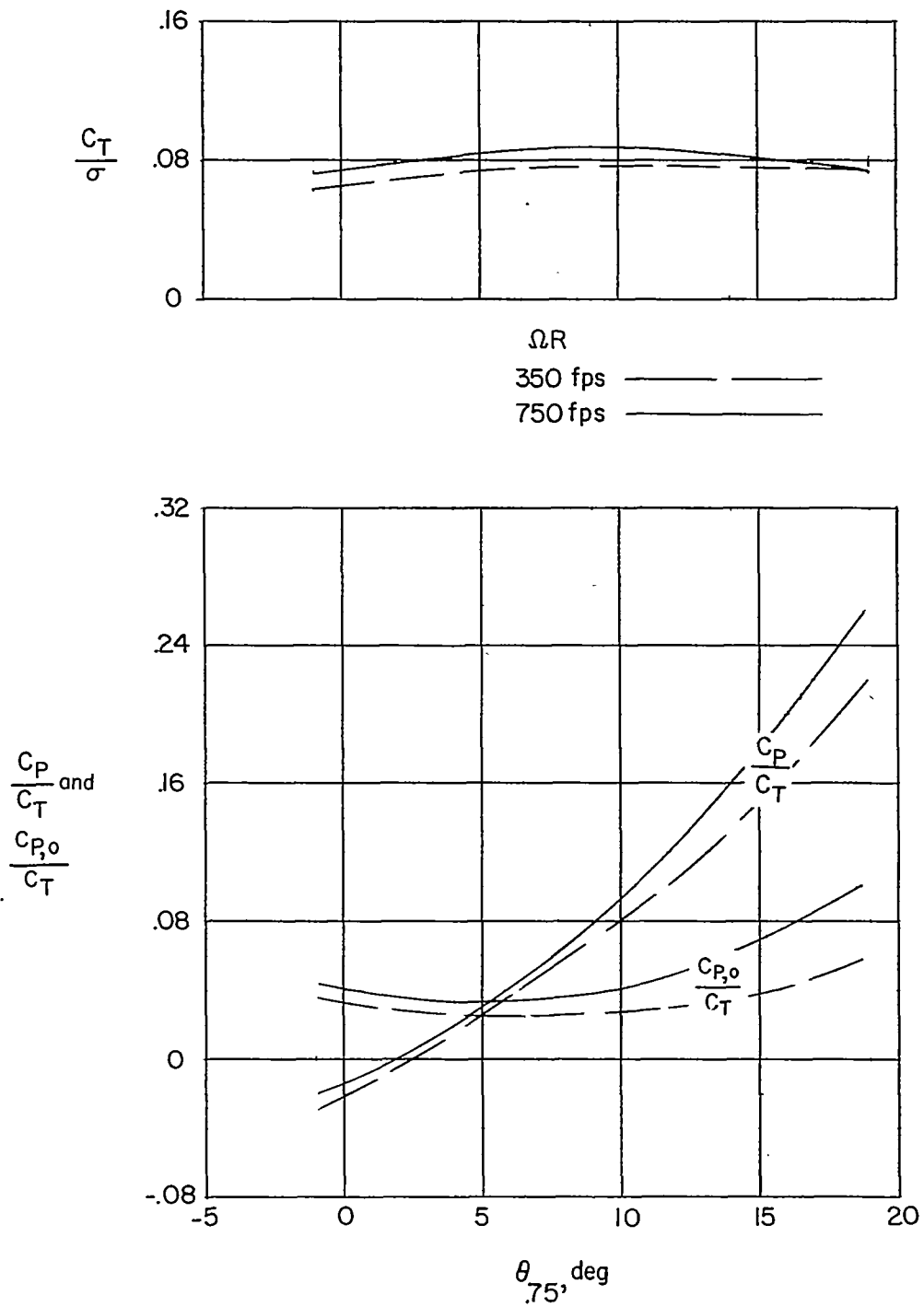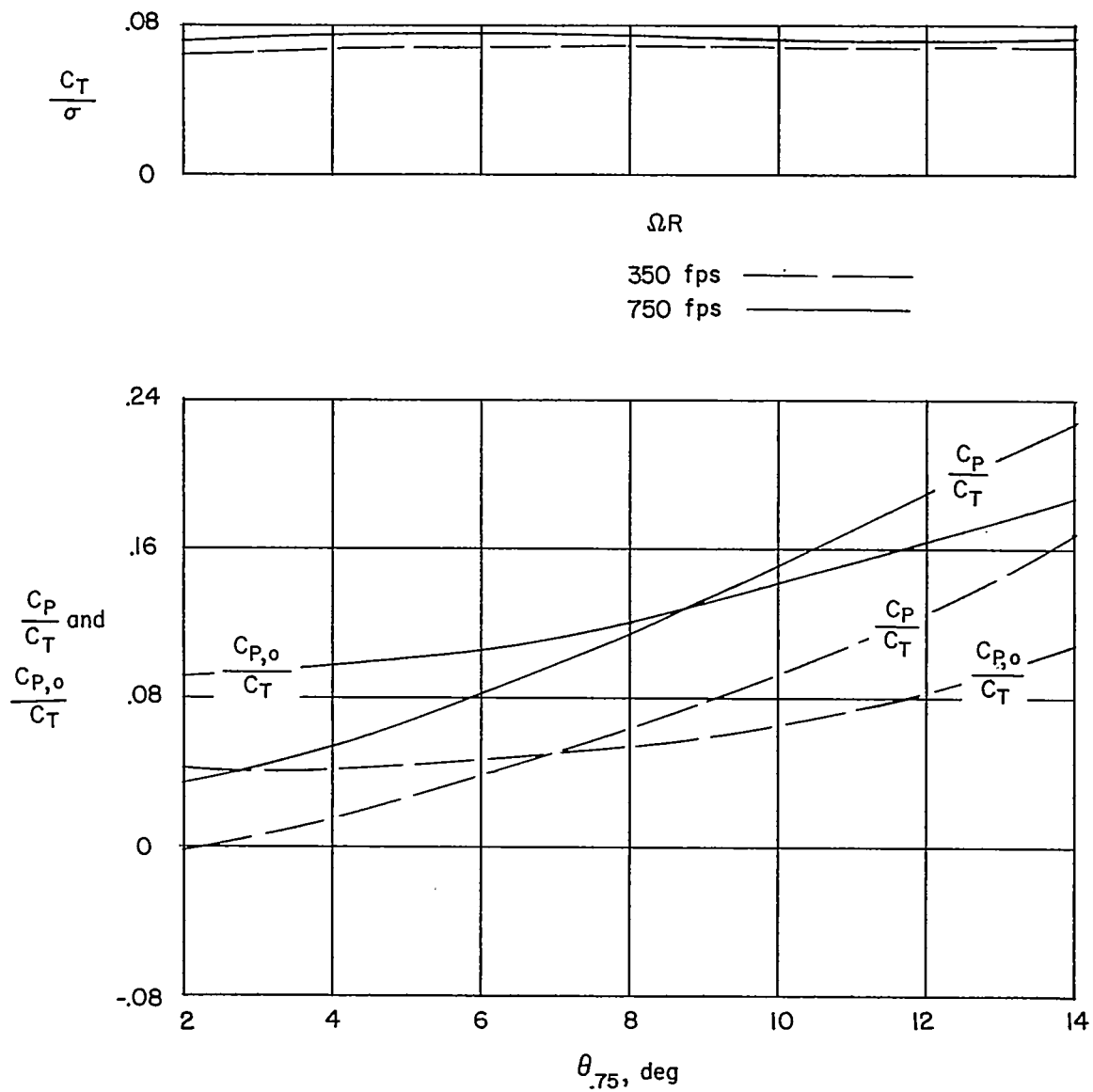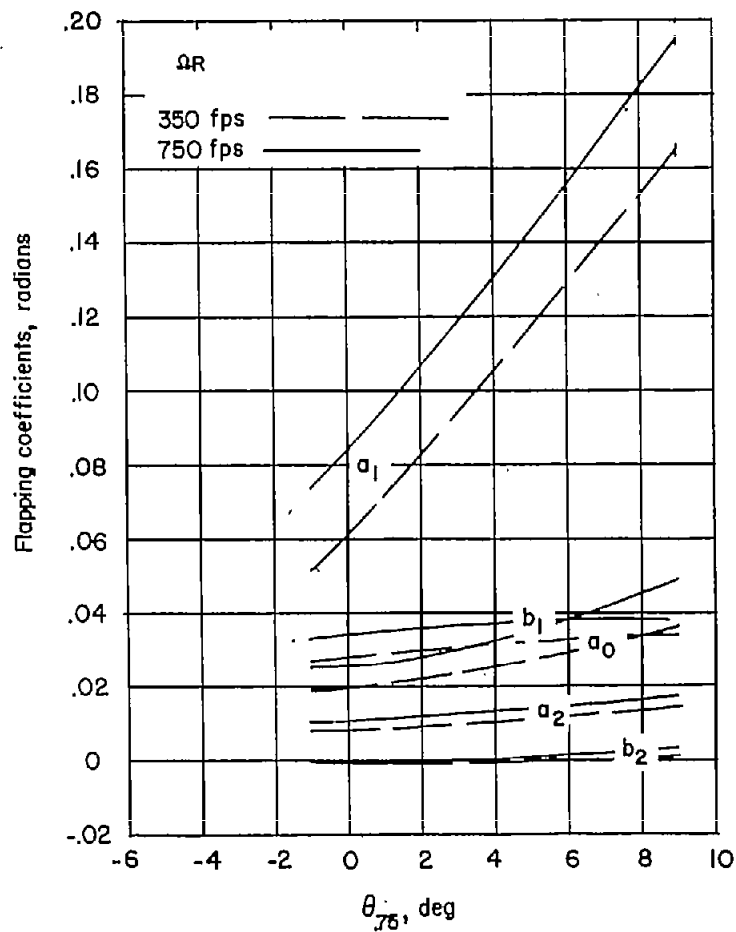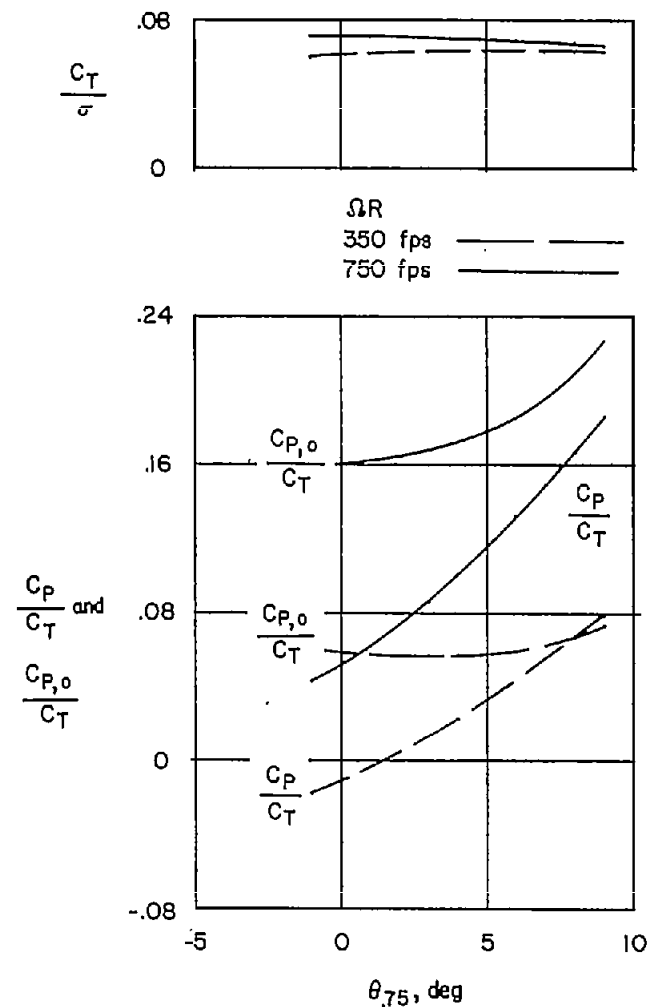
(b) Thrust and power coefficients.

Figure 2.- Concluded.
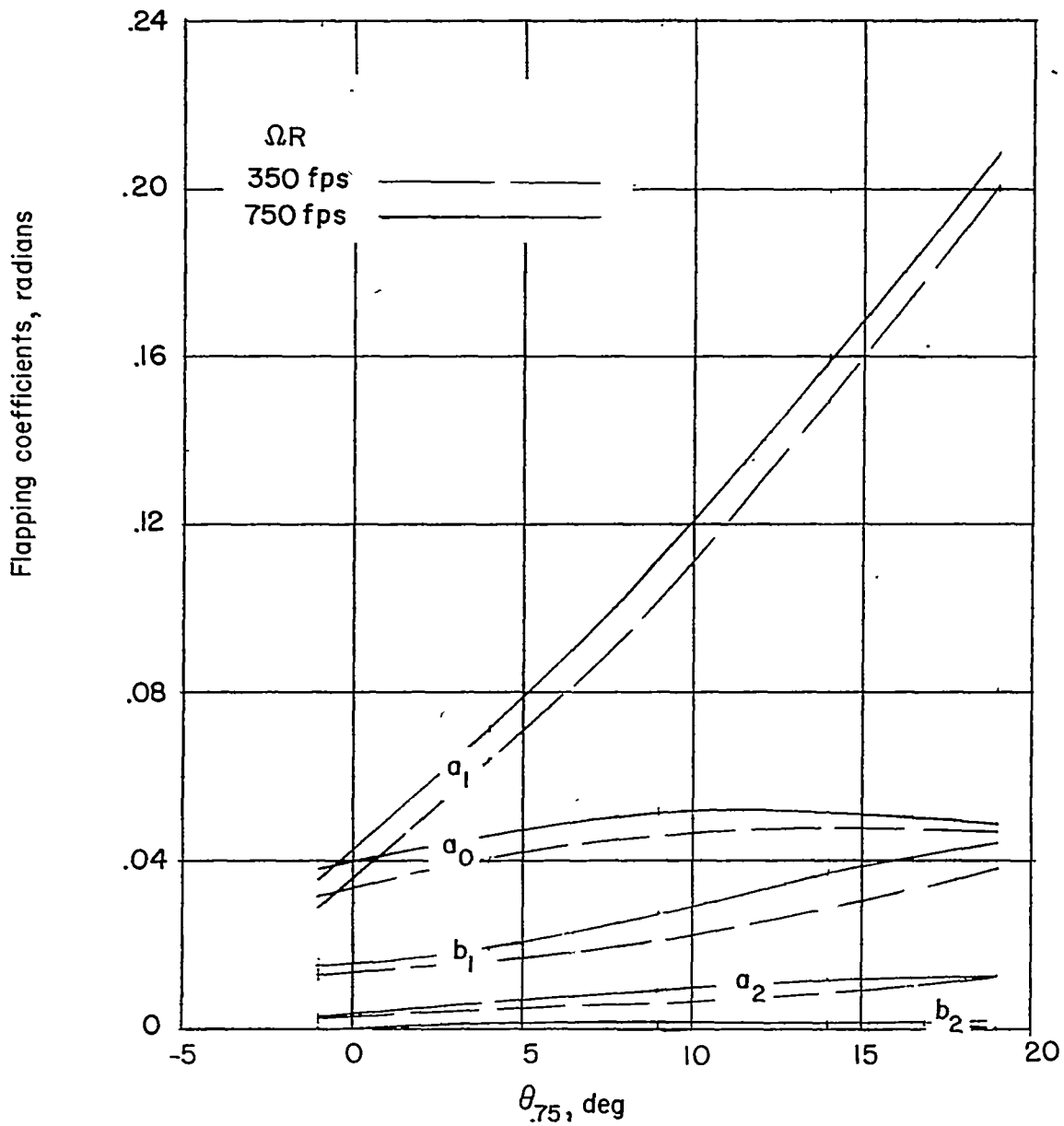
(a) Flapping coefficients.

Figure 3.- Aerodynamic effects of high-tip-speed operation
$\left(\mu = 0.3, \quad \theta_1 = -8^\circ\right)$.

ΩR

350 fps ——— ———

750 fps ———
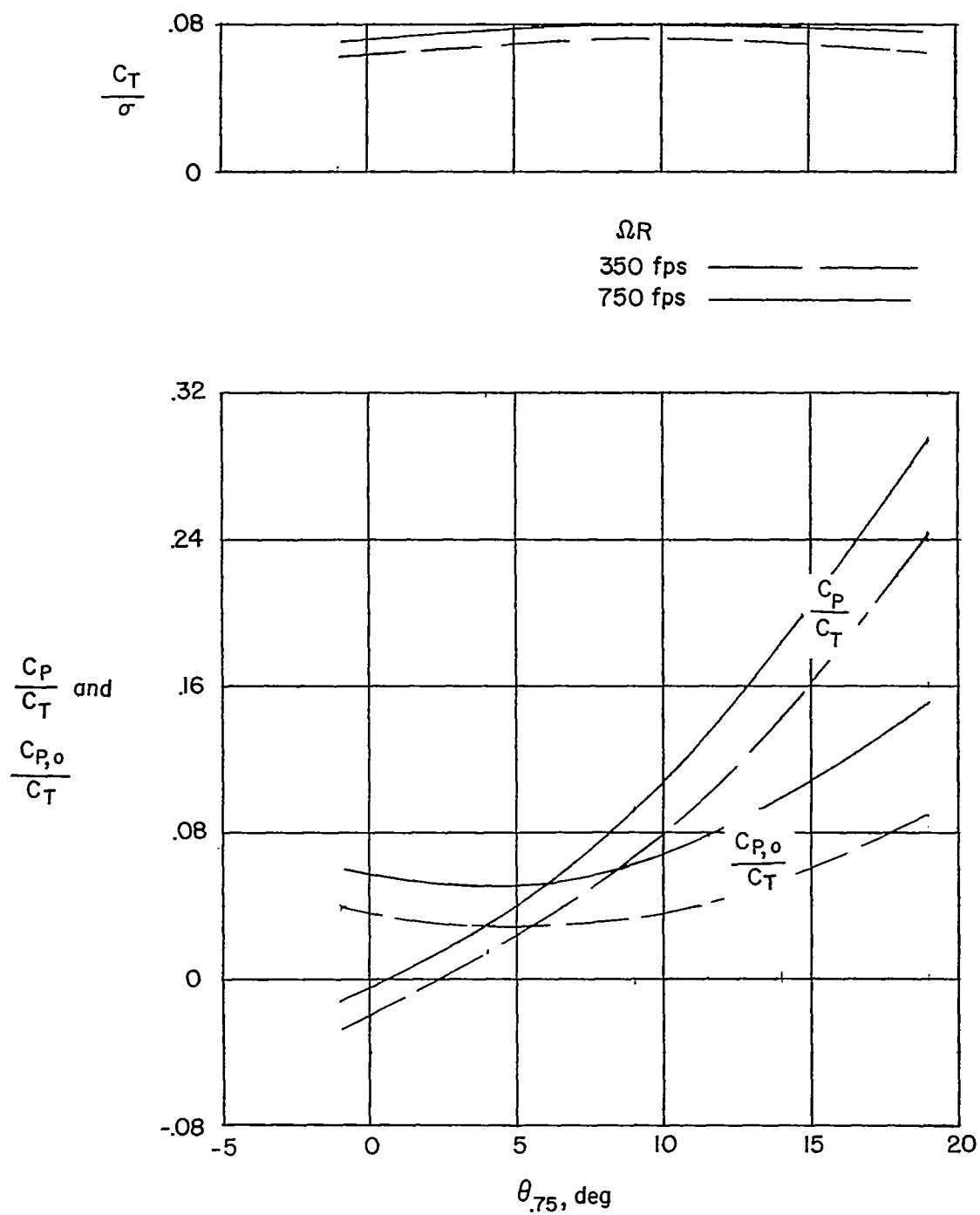
(b) Thrust and power coefficients.

Figure 3.- Concluded.
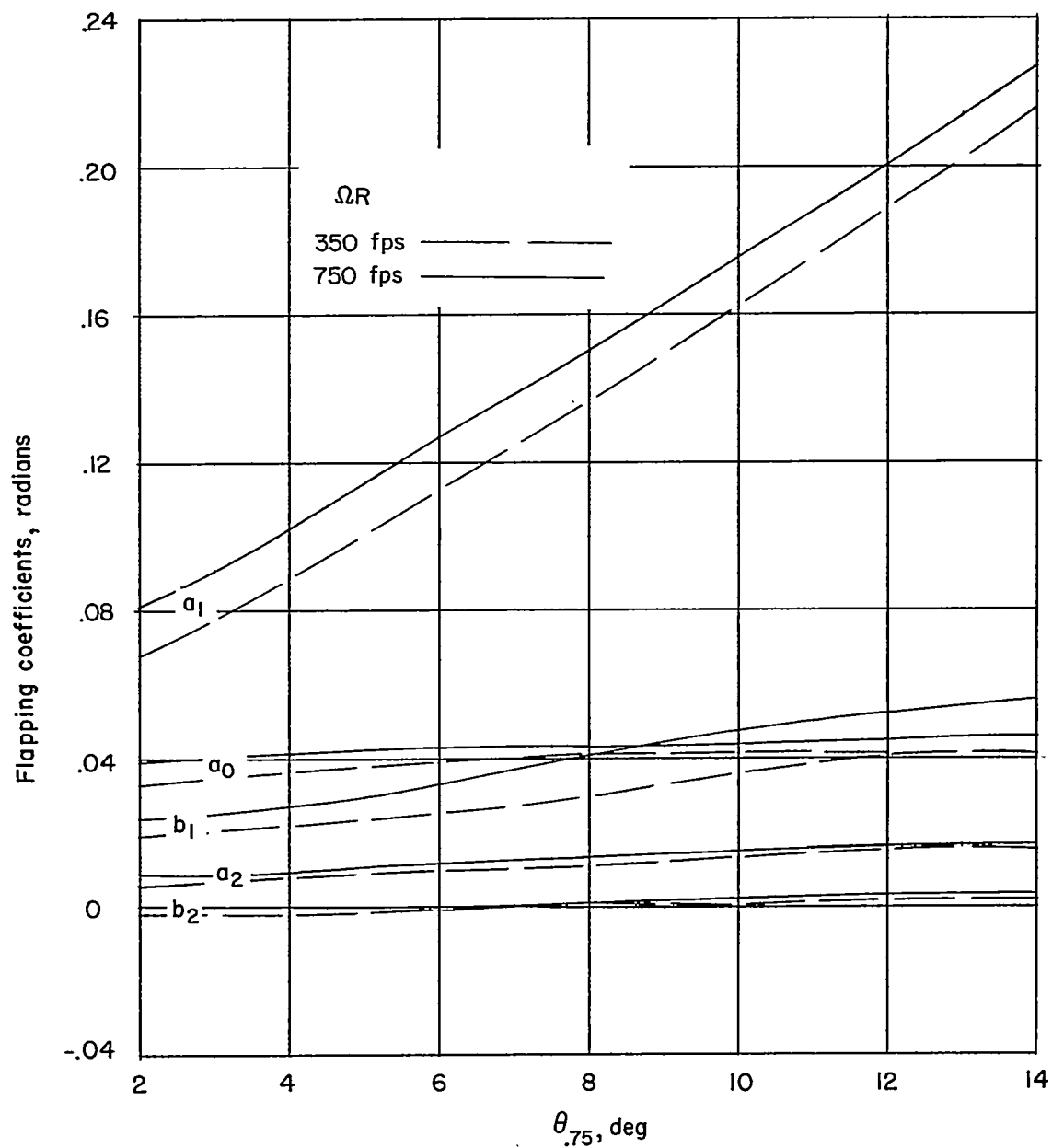
(a) Flapping coefficients.

Figure 4.- Aerodynamic effects of high-tip-speed operation
$\left(\mu = 0.4, \quad \theta_1 = -8°\right)$.

ΩR

350 fps — · — — · —

750 fps ———— ————

(b) Thrust and power coefficients.

Figure 4.- Concluded.

(a) Flapping coefficients.

(b) Thrust and power coefficients.

Figure 5.- Aerodynamic effects of high-tip-speed operation $\left(\mu = 0.5, \quad \theta_1 = -8°\right)$.
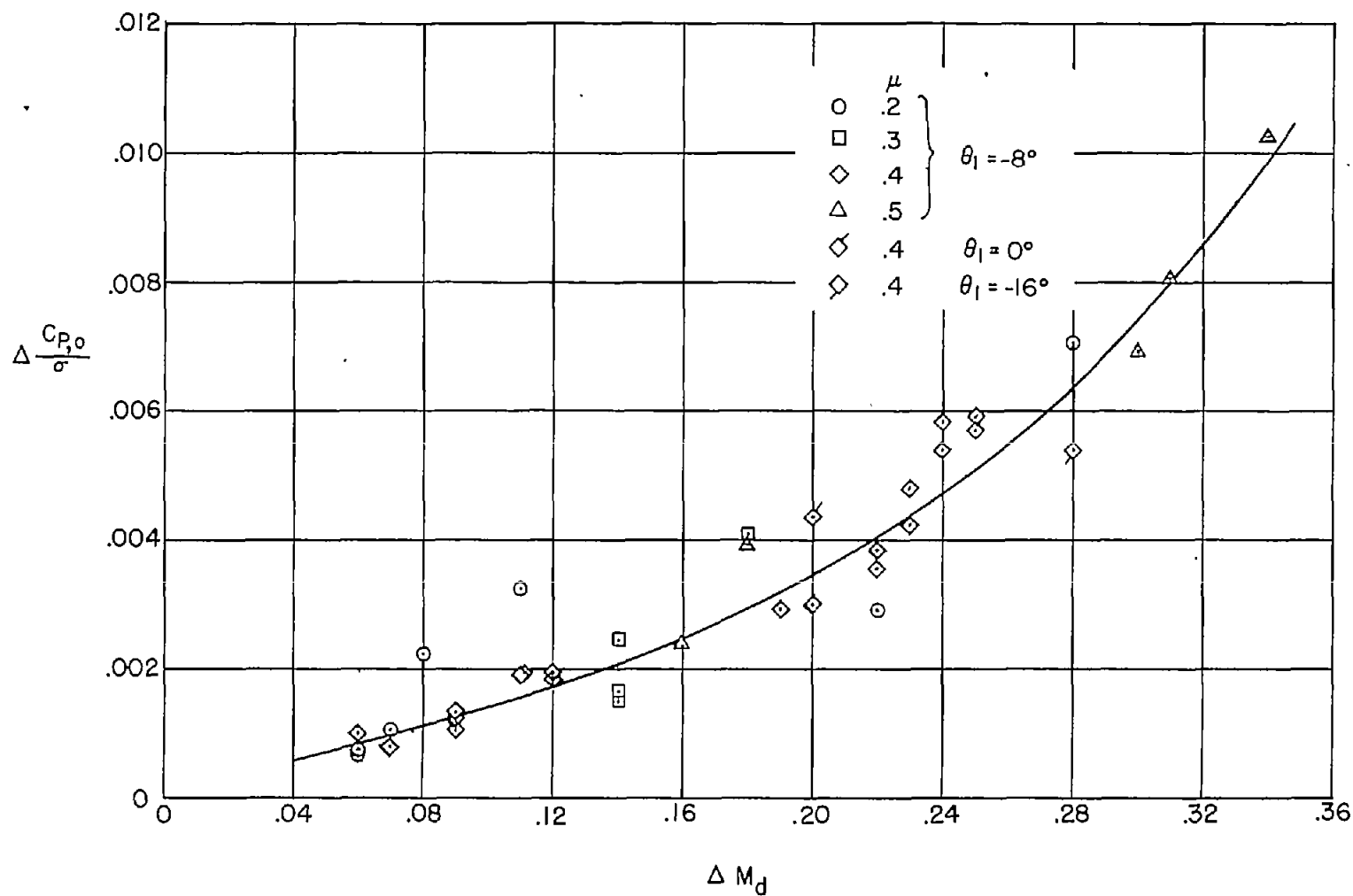
Figure 6.- Rotor profile-drag-coefficient increment (due to compressibility) as a function of the amount by which the drag-divergence Mach number is exceeded at the tip of the advancing blade.
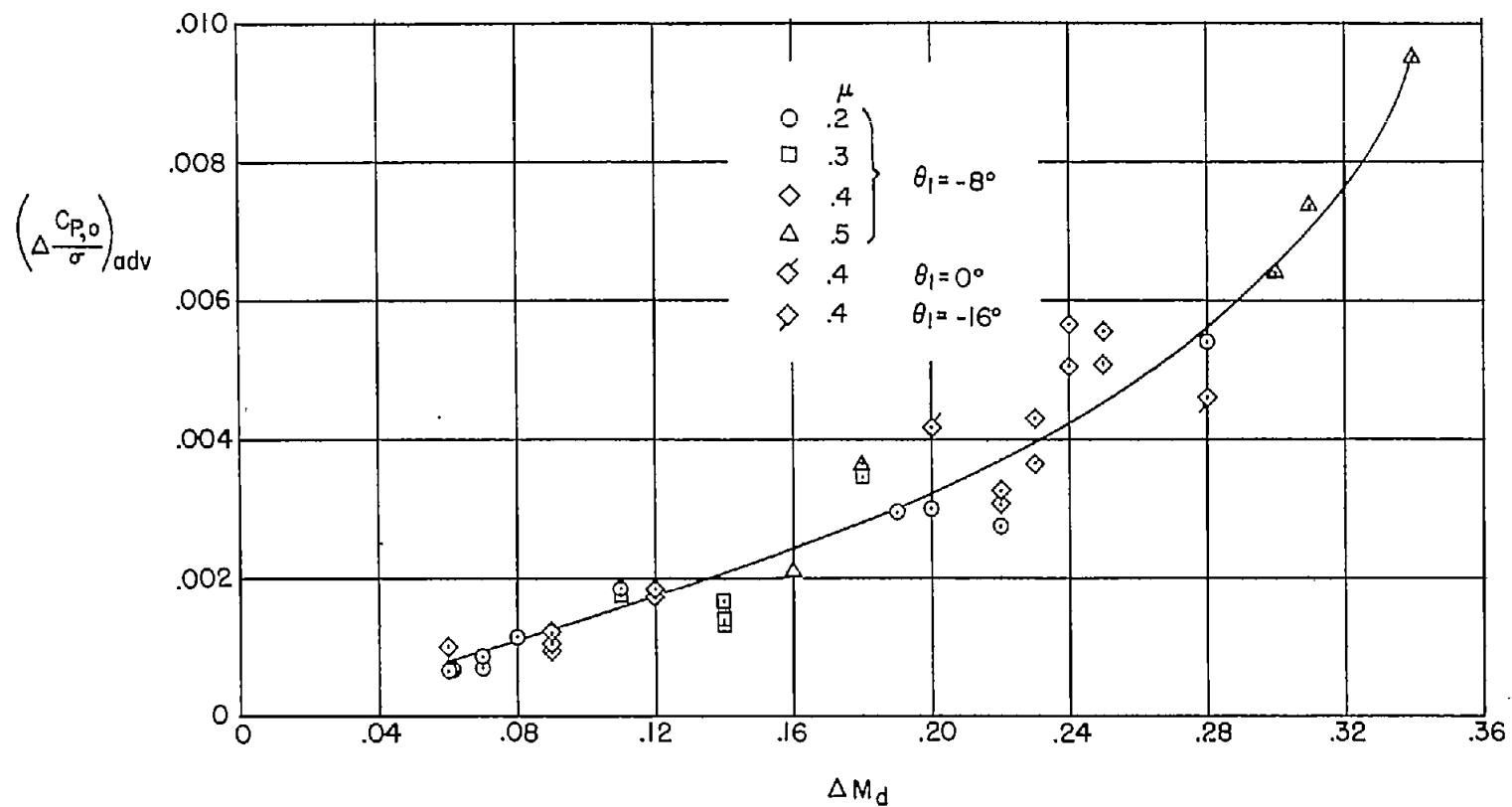
Figure 7.- Rotor profile-drag-coefficient increment (due to compressibility) for advancing side of disk as a function of the amount by which the drag-divergence Mach number is exceeded at the tip of the advancing blade.
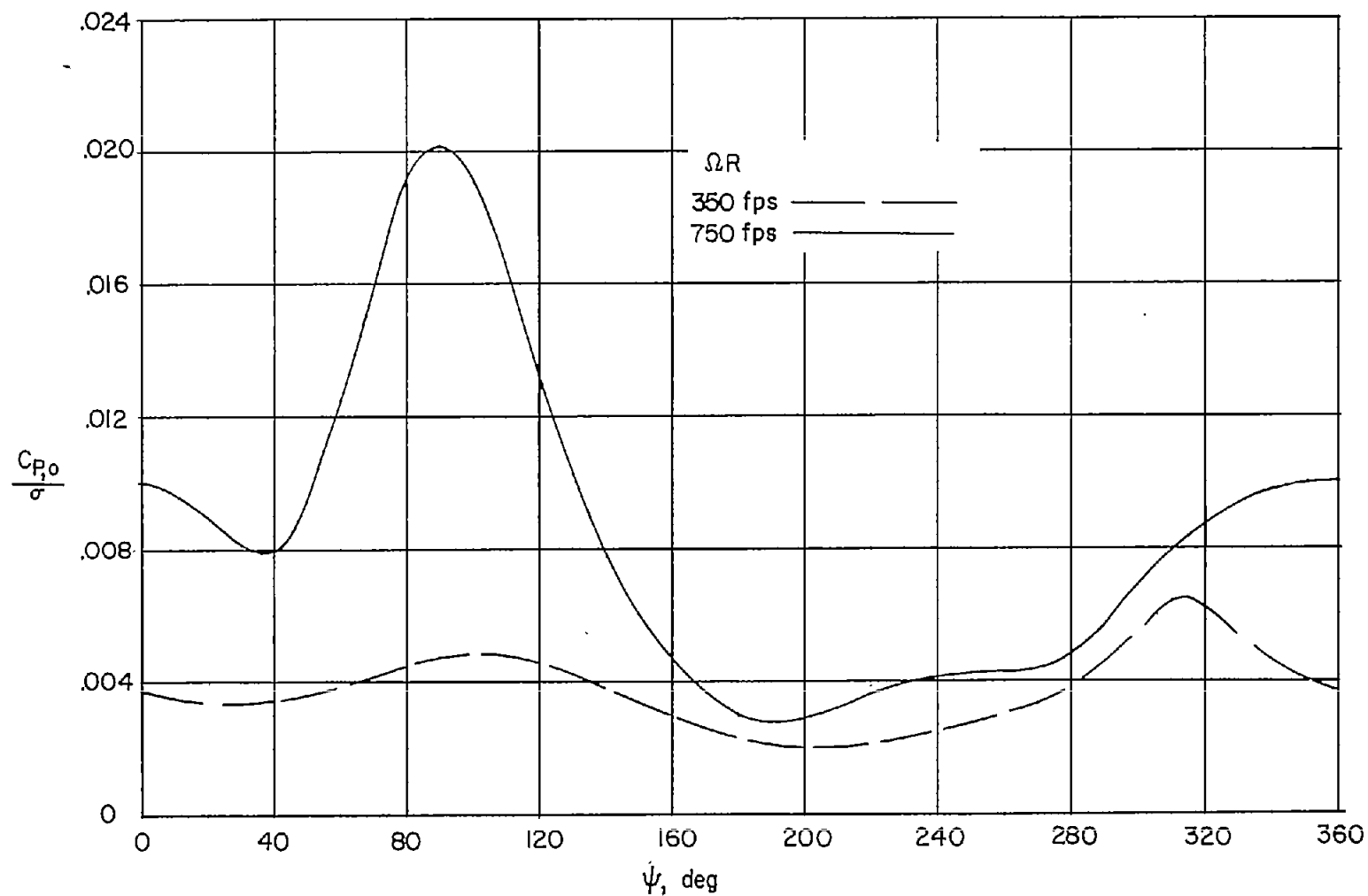
Figure 8.- Effects of compressibility on azimuth distribution of rotor profile-drag losses $\left(\mu = 0.4, \quad \lambda = -0.060, \quad \theta_{.75} = 8^{\circ}, \quad \theta_1 = -8^{\circ}\right)$.
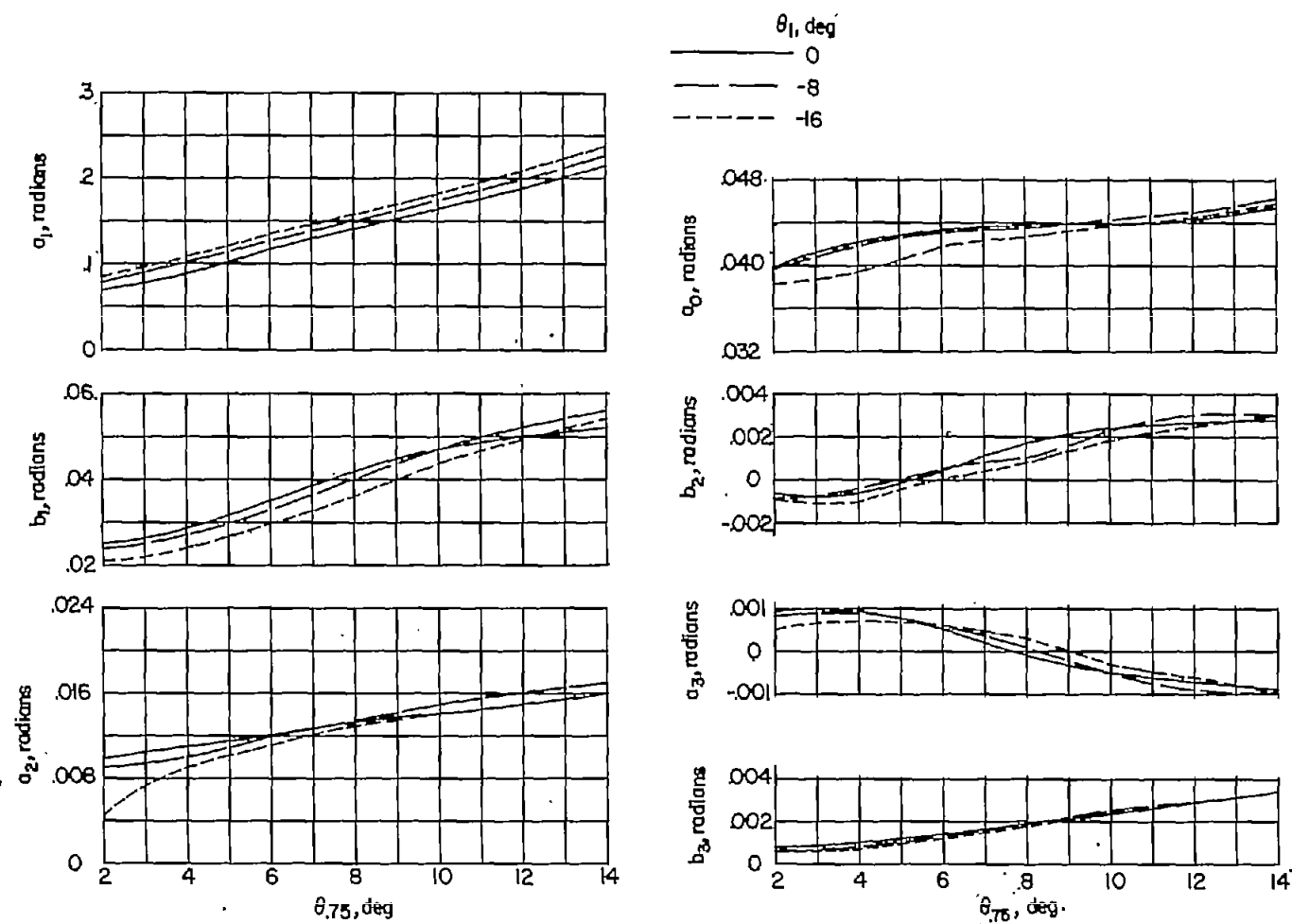
(a) Blade flapping coefficients.

Figure 9.- Effects of blade twist in operation at high tip speed
$\left(\mu = 0.4, \quad \Omega R = 750 \text{ fps}\right)$.
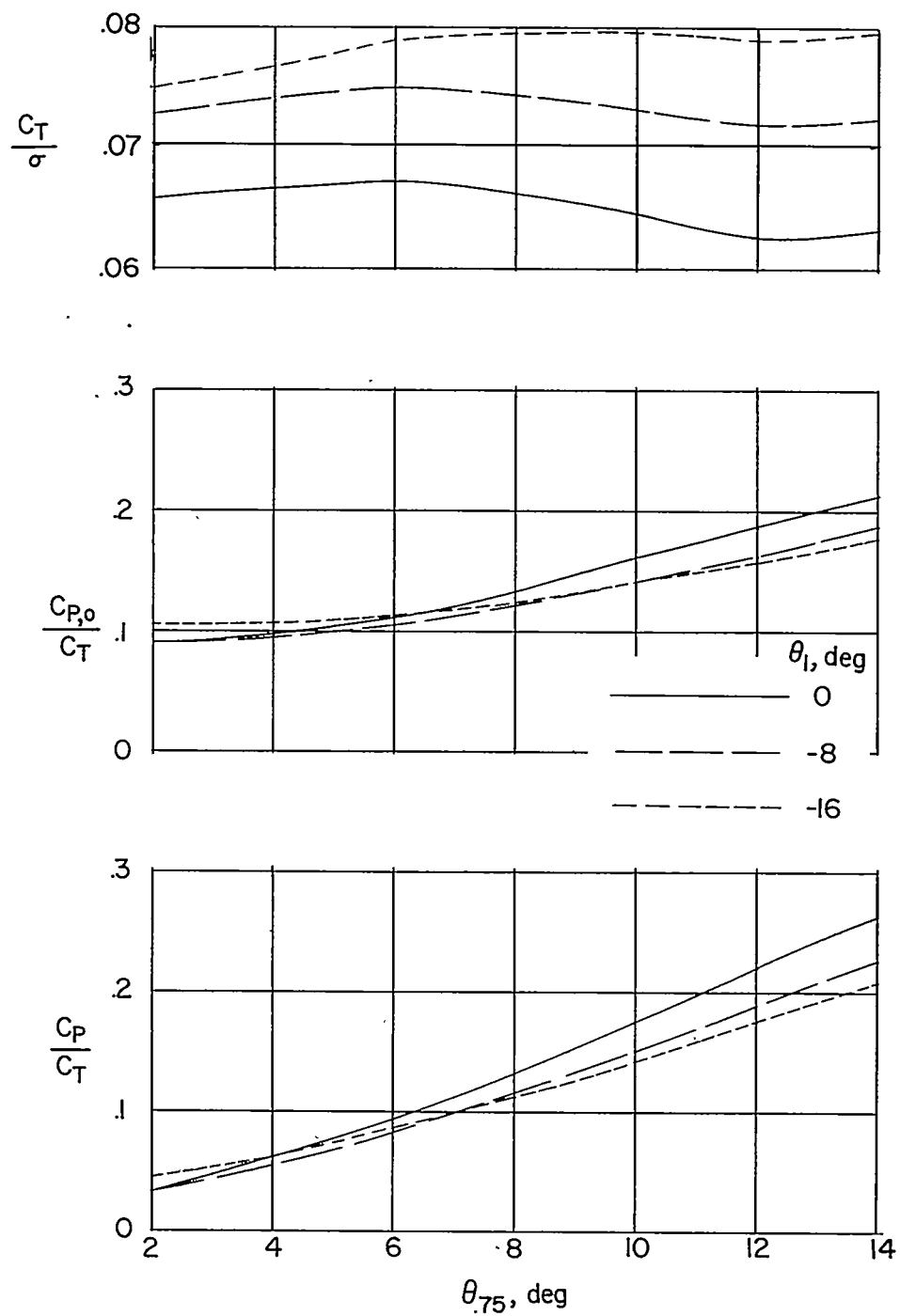
(b) Rotor thrust and power coefficients.

Figure 9.- Continued.
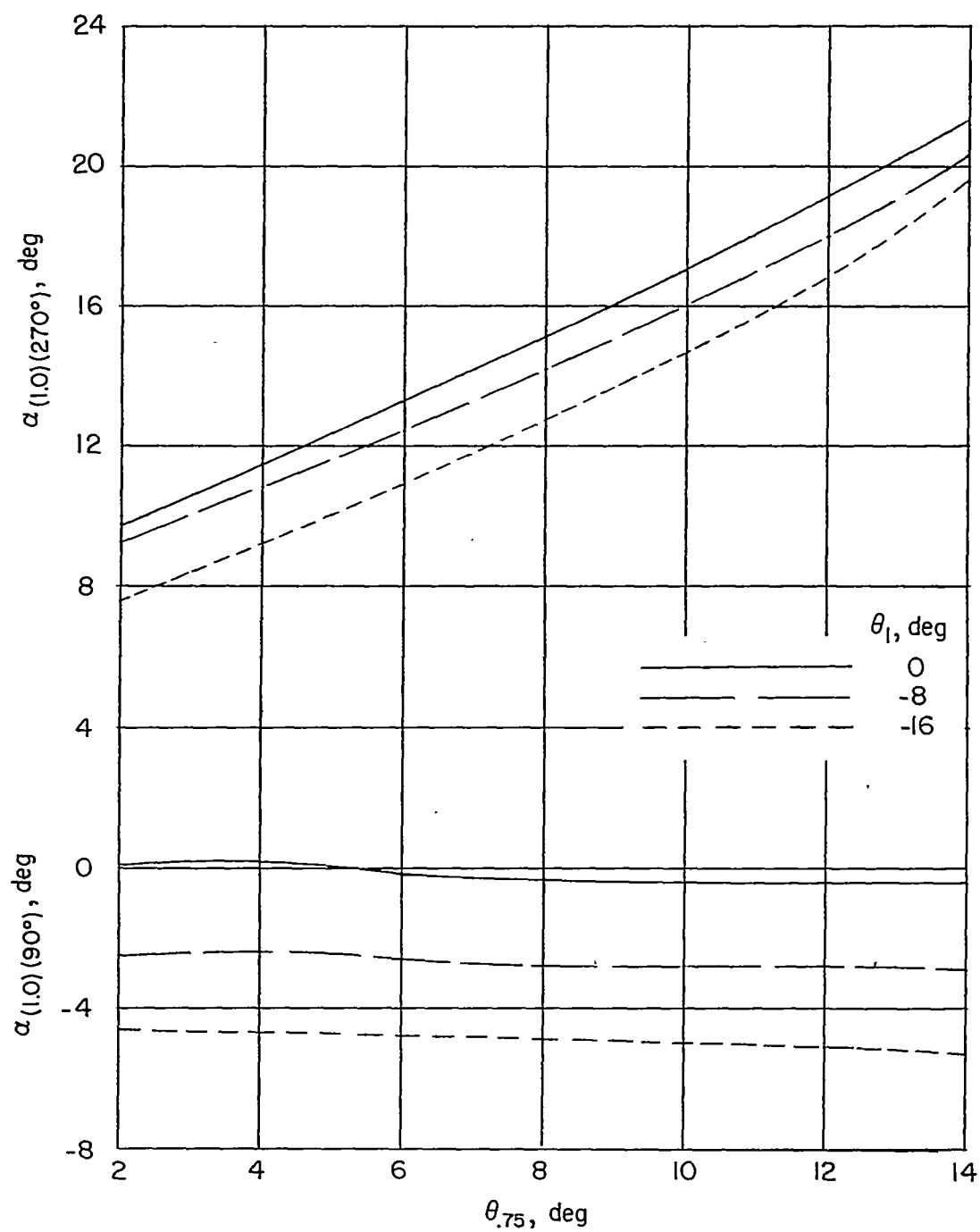
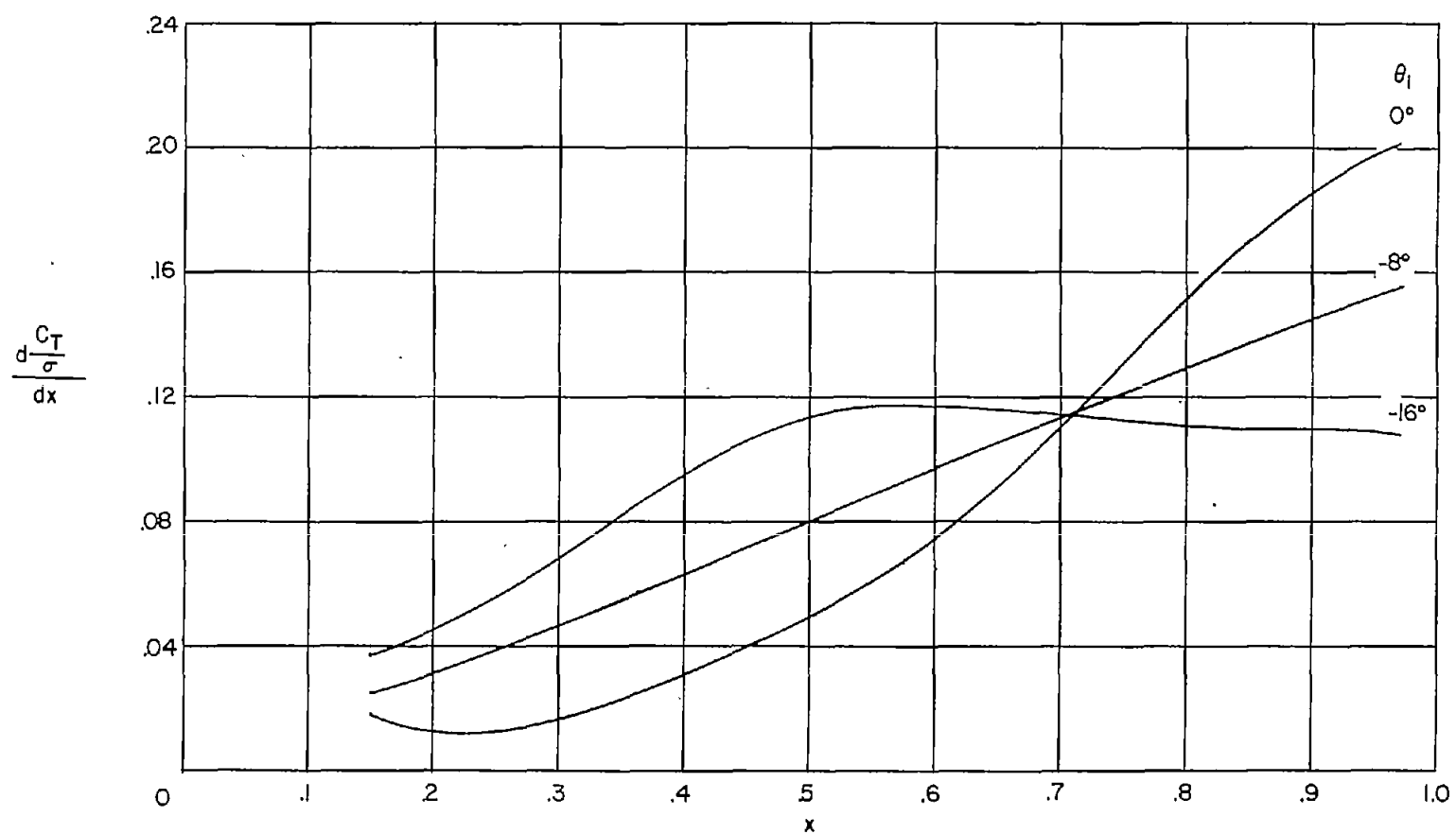(c) Advancing- and retreating-blade-tip angles of attack.

Figure 9.- Concluded.

Figure 10.- Effect of blade twist on radial thrust distribution at high-tip-speed operation $\left(\mu = 0.4, \quad \lambda = -0.060, \quad \theta_{.75} = 8°, \quad \Omega R = 750 \text{ fps}\right)$.
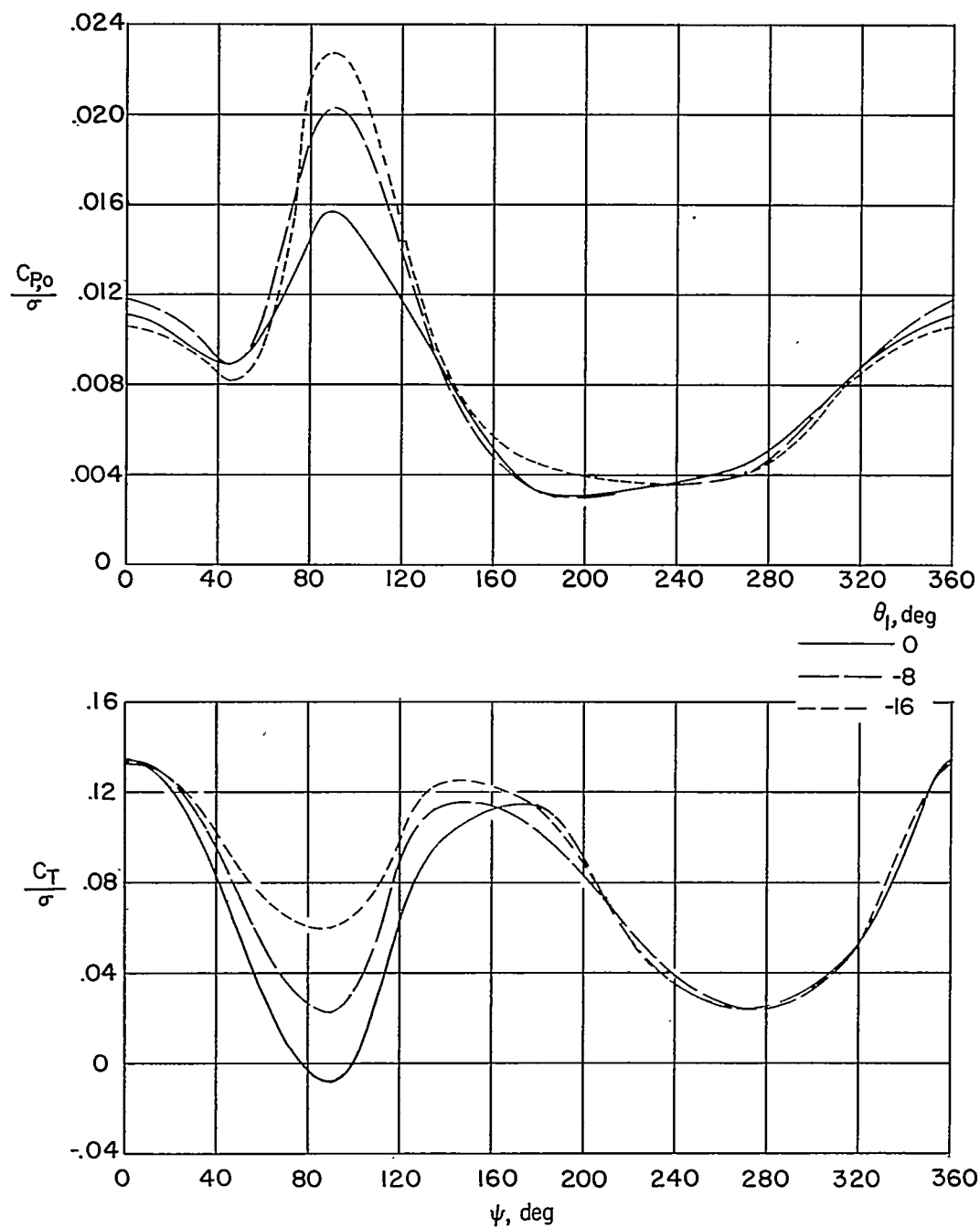
Figure 11.- Effect of blade twist on azimuth thrust and profile-power distribution at high-tip-speed operation $\left(\mu = 0.4, \quad \lambda = -0.060, \quad \theta_{.75} = 8°, \quad \Omega R = 750 \text{ fps}\right)$.
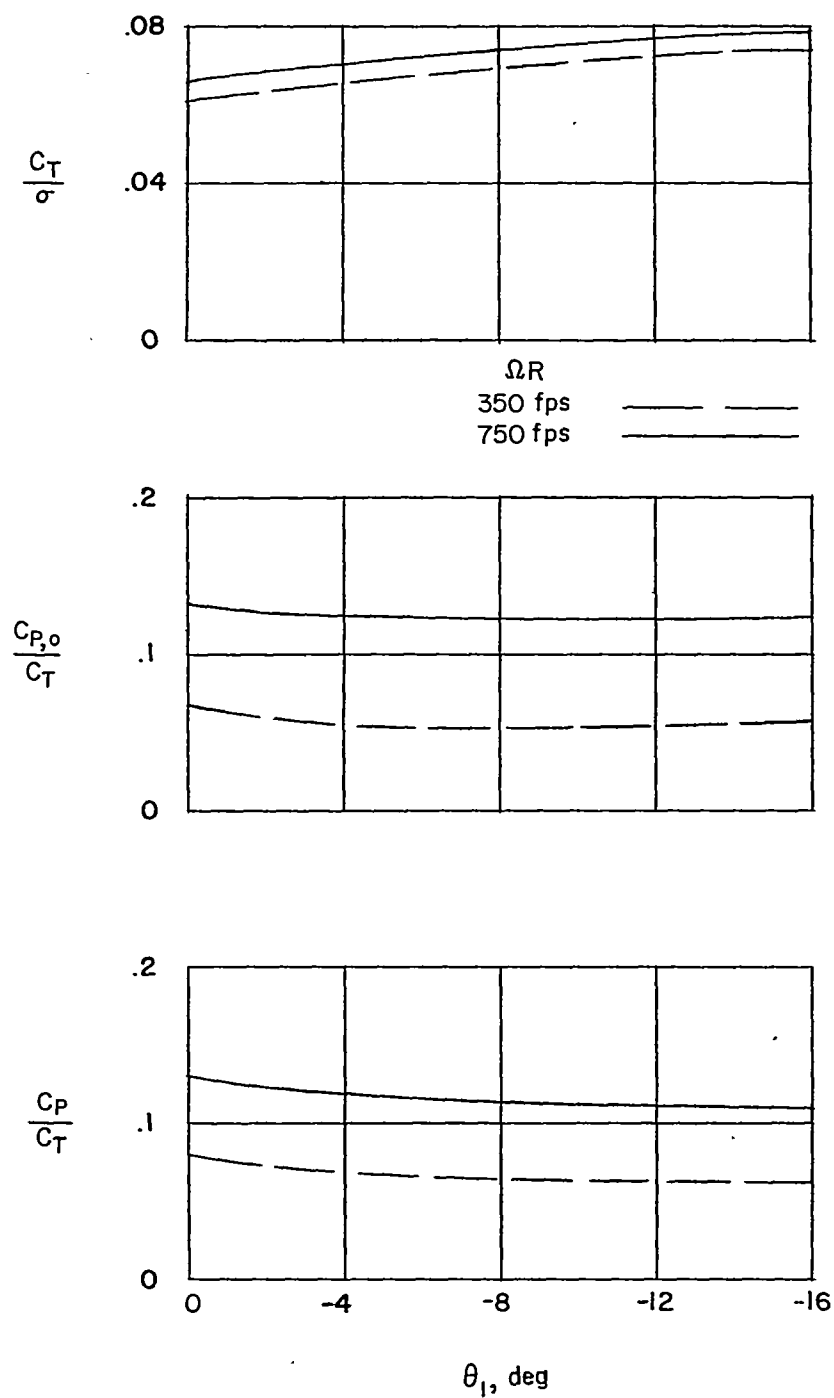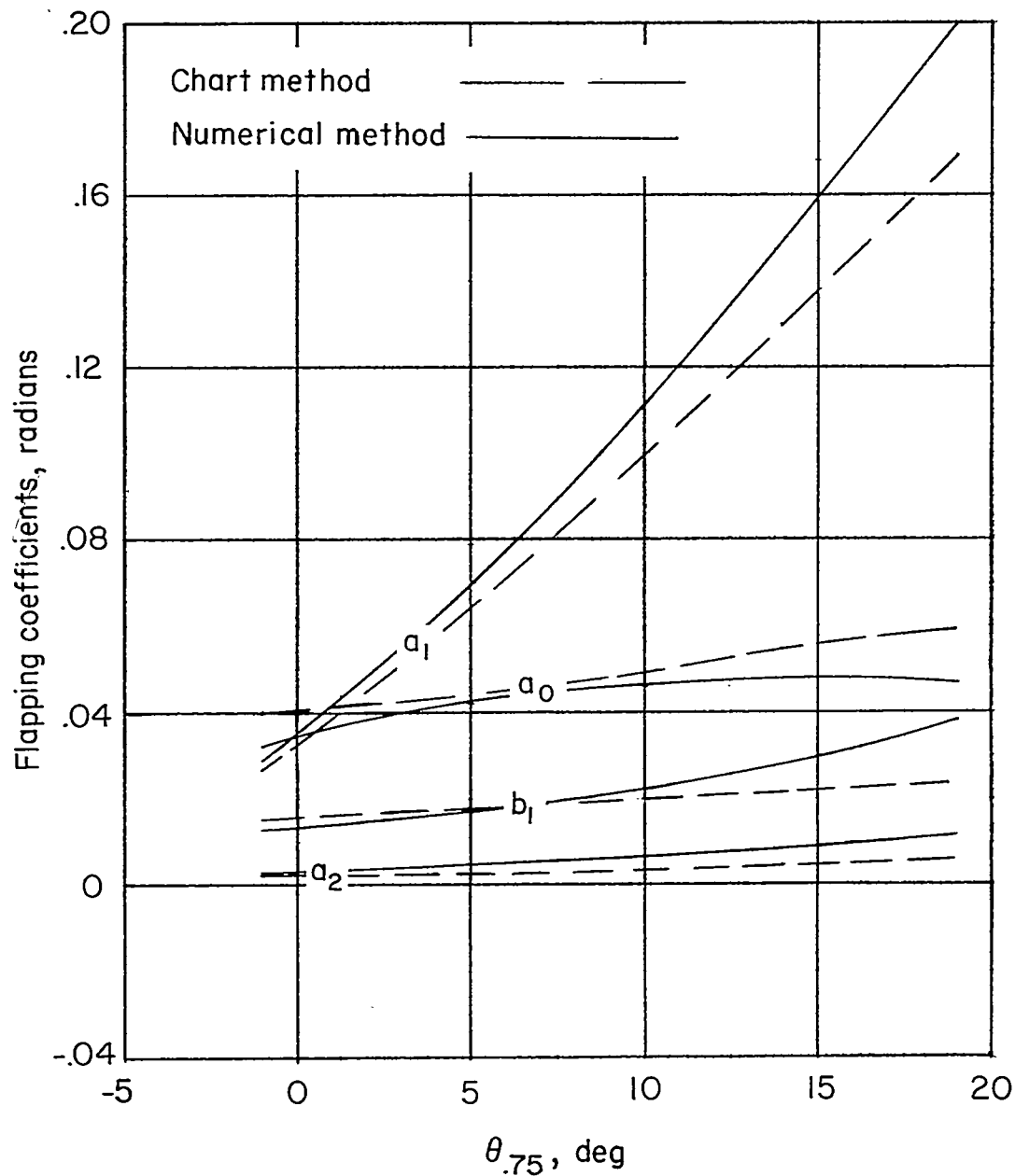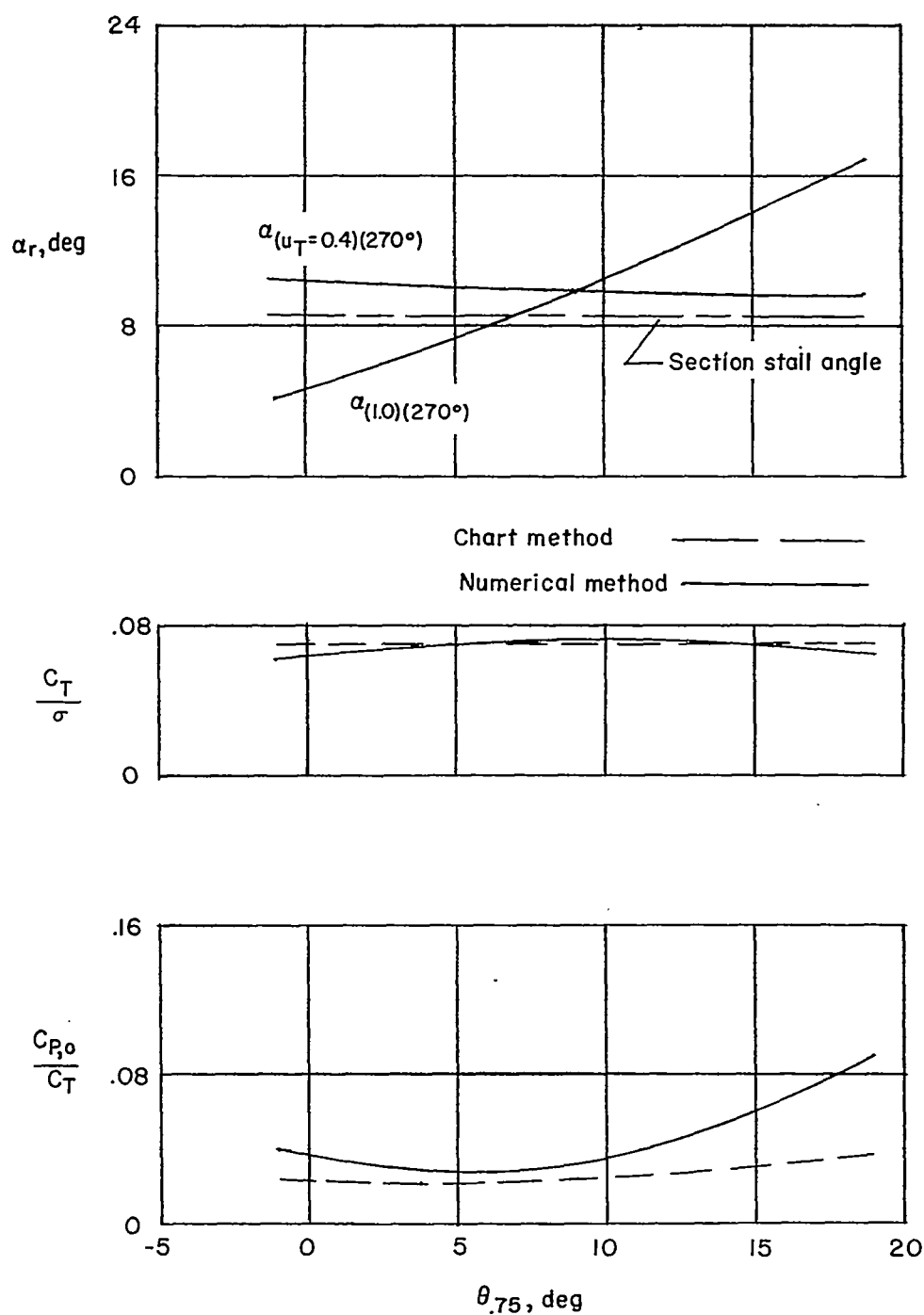
Figure 12.- Influence of blade twist on effects of compressibility on rotor thrust and power $\left(\mu = 0.4, \quad \lambda = -0.060, \quad \theta_{.75} = 8^{\circ}\right)$.

(a) Blade flapping coefficients.

Figure 13.- Comparison of rotor characteristics as calculated by
numerical method of this paper ($\Omega R = 350$ fps) with chart method
of reference 6 $\left(\mu = 0.3, \quad \theta_1 = -8°\right)$.

(b) Section angles of attack, rotor thrust, and power coefficients.

Figure 13.- Concluded.